Article

Cell Reports

Two Distinct Pathways Support Gene Correction by Single-Stranded Donors at DNA Nicks

Graphical Abstract

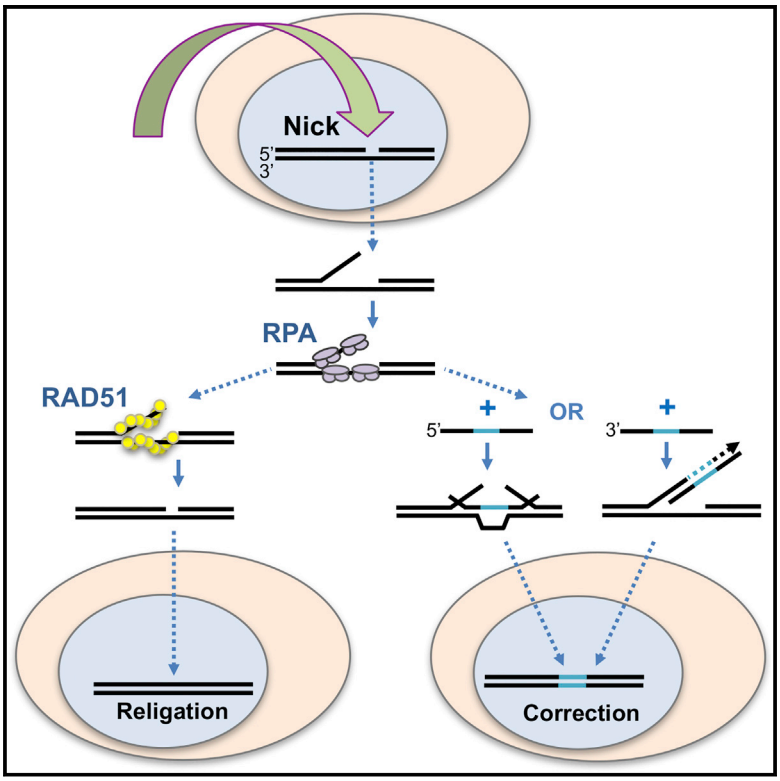

Authors

Luther Davis, Nancy Maizels

Correspondence

maizels@u.washington.edu

In Brief

Nicks are the most common form of DNA damage. Davis and Maizels define two distinct pathways that support homology-directed repair (HDR) at nicks and show that conserved factors suppress or promote genomic instability at nicks. This mechanistic understanding defines guidelines for design of efficient donors for gene correction.

Highlights

- Two pathways support HDR at nicks by ssDNA donors
- Mechanism-based design of donors improves gene correction efficiency
- RPA promotes both HDR and mutagenic end joining (mutEJ) at nicks
- RAD51 promotes genomic stability at nicks, suppressing both HDR and mutEJ

Davis & Maizels, 2016, Cell Reports *17*, 1872–1881
November 8, 2016 © 2016 The Author(s).
http://dx.doi.org/10.1016/j.celrep.2016.10.049

CellPress

OPEN ACCESS
CellPress

Cell Reports
Article

Two Distinct Pathways Support Gene Correction by Single-Stranded Donors at DNA Nicks

Luther Davis[1] and Nancy Maizels[1,2,3,4,*]
[1]Department of Immunology
[2]Department of Biochemistry
[3]Department of Pathology
University of Washington School of Medicine, Seattle, WA 98195, USA
[4]Lead Contact
*Correspondence: maizels@u.washington.edu
http://dx.doi.org/10.1016/j.celrep.2016.10.049

SUMMARY

Nicks are the most common form of DNA damage. The mechanisms of their repair are fundamental to genomic stability and of practical importance for genome engineering. We define two pathways that support homology-directed repair by single-stranded DNA donors. One depends upon annealing-driven strand synthesis and acts at both nicks and double-strand breaks. The other depends upon annealing-driven heteroduplex correction and acts at nicks. Homology-directed repair via these pathways, as well as mutagenic end joining, are inhibited by RAD51 at nicks but largely independent of RAD51 at double-strand breaks. Guidelines for coordinated design of targets and donors for gene correction emerge from definition of these pathways. This analysis further suggests that naturally occurring nicks may have significant recombinogenic and mutagenic potential that is normally inhibited by RAD51 loading onto DNA, thereby identifying a function for RAD51 in maintenance of genomic stability.

INTRODUCTION

DNA nicks are the most common form of DNA damage, but the potential of DNA nicks to contribute to genomic instability was overlooked for considerable time because nicks were presumed to undergo immediate religation. This view was challenged when it became possible to compare outcomes of DNA nicks and double-strand breaks (DSBs) targeted to specific sites in genomic DNA by nickase derivatives of sequence-specific endonucleases. Using the homing endonuclease I-AniI and its nicking derivative I-AniI^{K227M}, we showed that nicks can initiate efficient homology-directed repair (HDR) accompanied by relatively little local mutagenesis (Davis and Maizels, 2011, 2014). A nick can be converted to a DSB in S phase, but the mechanism of HDR at nicks was readily distinguished from that of HDR at DSBs by characteristic strand asymmetries in the response to transcription and efficiencies of repair by single-stranded DNA donors (Davis and Maizels, 2014). Surprisingly, inhibition of RAD51 or of BRCA2 stimulated HDR at nicks by single-stranded donors 10-fold or more, achieving efficiencies comparable to that of HDR by duplex DNA donors at DSBs (Davis and Maizels, 2014).

RAD51 is essential for HDR at DSBs by duplex DNA donors. In mammalian cells, 5′–3′ resection exposes single-stranded 3′ ends of a DSB, RPA coats the single-stranded regions, then BRCA2 promotes loading of RAD51 to enable strand invasion of the donor duplex (Heyer et al., 2010; Symington and Gautier, 2011; Kowalczykowski, 2015). The evidence that RAD51 normally inhibits HDR at nicks by single-stranded DNA donors raised the possibility that HDR can proceed by an alternative pathway distinct from canonical HDR. This alternative pathway has physiological implications, particularly for tumors deficient in canonical HDR, and it is also of interest for genome engineering applications, for which single-stranded deoxyoligonucleotide (SSO) donors are superior to duplex donors in many respects.

Initial characterization of gene correction by SSO donors showed that donors complementary to either the intact (cI) or nicked (cN) strand can support HDR (Davis and Maizels, 2014). We proposed that cN donors anneal to the 3′ end of the nicked target and template repair synthesis, and cI donors anneal to form a heteroduplex that spans the region to be corrected and convert the target sequence either by mismatch repair or during the next round of replication (Figure 1A). Here, we provide experimental support for that proposal. We demonstrate that the 3′ end of the nicked target primes repair DNA synthesis using a cN donor as template, resulting in unidirectional sequence conversion. In contrast, a cI donor anneals to the target enabling conversion of markers on either side of the nick. We show that RPA, which coats single-stranded DNA (ssDNA) to prevent reannealing (Chen and Wold, 2014; Deng et al., 2015), promotes both gene correction and mutagenic end-joining (mutEJ) at nicks. We show that HDR at nicks by SSO donors is stimulated by depletion of RAD51 or of BRCA2, PALB2, or DSS1, which load RAD51 onto DNA, but HDR at DSBs by SSO donors is independent of these factors. These experiments provide guidelines for coordinated design of targets and donors for gene correction at DNA nicks. They further establish that nicks have the potential to initiate recombination and local mutagenesis, via pathways stimulated by RPA, and RAD51 opposes these outcomes to promote genomic stability at nicks.

This is an open access article under the CC BY-NC-ND license (http://creativecommons.org/licenses/by-nc-nd/4.0/).

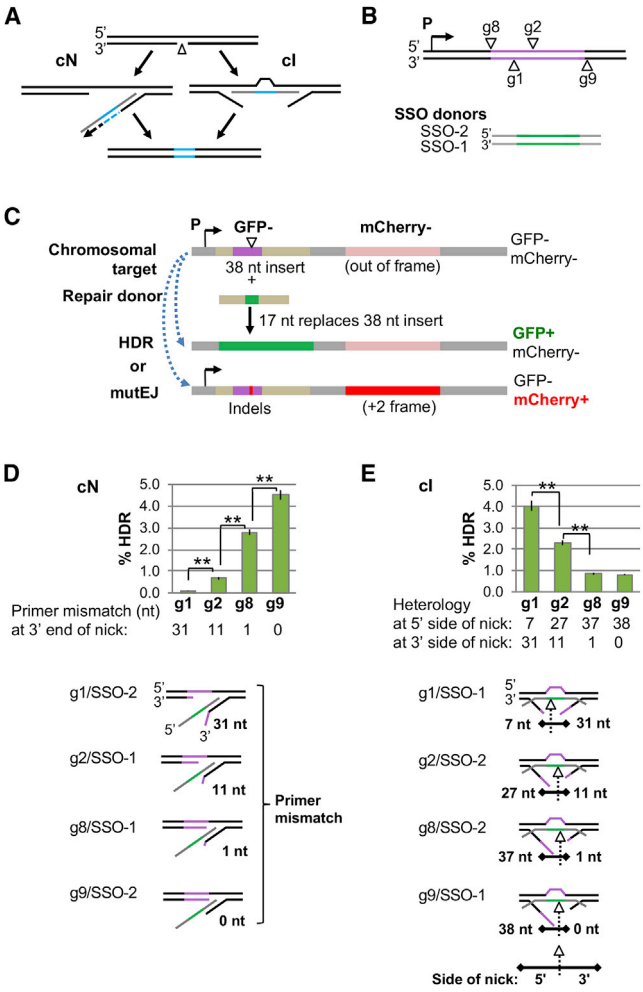

Figure 1. SSO Donor Strand and Target Site Preference of HDR at Nicks

(A) Diagram of HDR at a nick by an SSO donor complementary to the intact (cI) or nicked (cN) target strand. Top line, nicked DNA. Middle line, annealed cI (left) and cN (right) donors, with sequence to be transferred shown in blue and donor homology arms in gray. Bottom line, products of HDR.

(B) Diagram of the TL reporter, showing the promoter (P), the central 37-bp heterologous region (purple) the positions of nicks targeted by gRNAs 1, 2, 8, and 9 (arrowheads), and the 99 nt SSO-1 and SSO-2 donors carrying a central 17-nt region (green) that must replace the heterologous region to enable GFP$^+$ expression.

(C) TL reporter assay of HDR and mutEJ, showing chromosomal target bearing promoter (P), defective GFP gene and out of frame mCherry gene. Targeted nick (arrowhead) initiates repair by an HDR donor that enables GFP+ expression, or mutEJ (indels) that enable mCherry$^+$ expression.

(D) Top: HDR frequencies supported by cN donors at nicks targeted by indicated guide RNAs. Primer mismatch of the target/donor is indicated. HDR was stimulated by knockdown of BRCA2. HDR frequencies are shown as mean and SEM (SEM, n = 6, **p < 10^{-3}, raw data presented in Data S1). Bottom: postulated intermediates formed by annealing of cN donors to nicks at each target site. Extent of primer mismatch between the 3′ end of the target and donor is shown. See also Figure S1.

(E) As in (D), but HDR was supported by cI donors, and extent of heterology at the 5′ and 3′ sides of the nick are indicated. Postulated intermediates formed by annealing of cI donors are shown, and extent of heterology between the donor and the 5′ and 3′ sides of the nicks is indicated.

RESULTS

Distinct Homology Requirements for SSO Donors Complementary to the Nicked or the Intact Strand

The model for gene correction by SSO donors that we previously proposed (Figure 1A) requires that both cN and cI donors anneal to the target, a process that may be limited if insufficient ssDNA is exposed by unwinding or resection of the regions of the target 3′ or 5′ of the nick. In addition, it makes distinct predictions for cN and cI donors. For cN donors, (1) efficient HDR will require the very 3′ end of the nick to prime synthesis using the donor as template, so minimizing 3′ heterology will increase HDR frequencies, and (2) sequences transferred will derive solely from the 5′ arm of the donor. For cI donors, (1) efficient HDR will depend upon annealing to the target to span the heterology, and annealing may be limited by the extent to which the intact strand has been exposed by unwinding/resection, and (2) sequences transferred by a cI donor may derive from either the 5′ or 3′ arm of the donor.

To test these predictions, we first compared the efficiency of HDR initiated by nicks targeted by the Cas9^{D10A} nickase derivative of the RNA-guided Cas9 endonuclease (Gasiunas et al., 2012; Jinek et al., 2012; Cong et al., 2013; Mali et al., 2013) to four different closely spaced sites in the Traffic Light (TL) reporter (Certo et al., 2011). The TL reporter has two distinct fluorescence outputs that enable scoring of HDR and mutEJ events as GFP$^+$ and mCherry$^+$ cells, respectively. HDR by a 17-bp heterologous donor sequence will convert a 38-bp insert within the defective GFP coding sequence to enable GFP expression, and the fraction of mutEJ events that cause a shift to the +2 reading frame enable mCherry$^+$ expression (Figure 1B). HDR was supported by two 99-nt donors, SSO-1 and SSO-2, complementary to one another and consisting of 41 nt homology arms flanking a central 17-nt region that is heterologous with the TL target (Figure 1C). We assayed HDR frequencies in HEK293T cells carrying the chromosomal TL reporter and treated with a non-targeting control small interfering RNA (siRNA), siNT2, or with siBRCA2, because we had previously discovered that inhibition of canonical HDR by depletion of BRCA2 or RAD51 greatly increased the efficiency of HDR at nicks by SSO donors (Davis and Maizels, 2014).

HDR frequencies supported by guide RNA/donor pairs that utilize the cN pathway at nicks (guide RNAs g2 or g8 and SSO-1; g1 or g9 and SSO-2; Figure 1B) varied over a 40-fold range (0.1%–4.5%; Figure 1D) in cells treated with siBRCA2. HDR frequencies increased as heterology between the donor and the 3′ end of the nick that primes new DNA synthesis decreased. The lowest frequency, 0.1%, was at the nick targeted by g1, where the extent of mismatch with the primer is 31 nt; and the highest frequency, 4.5%, was at the nick targeted by g9, at which there is no primer mismatch. A similar trend was evident in cells treated with the siNT2 control siRNA rather than siBRCA2, in which HDR frequencies were considerably lower (Figure S1A). These results support the hypothesis that cN donors anneal to the 3′ end of the nick, which primes repair synthesis using the donor as template. They highlight the importance of avoiding primer mismatch when designing SSO donors for gene correction via this annealing-driven strand synthesis pathway.

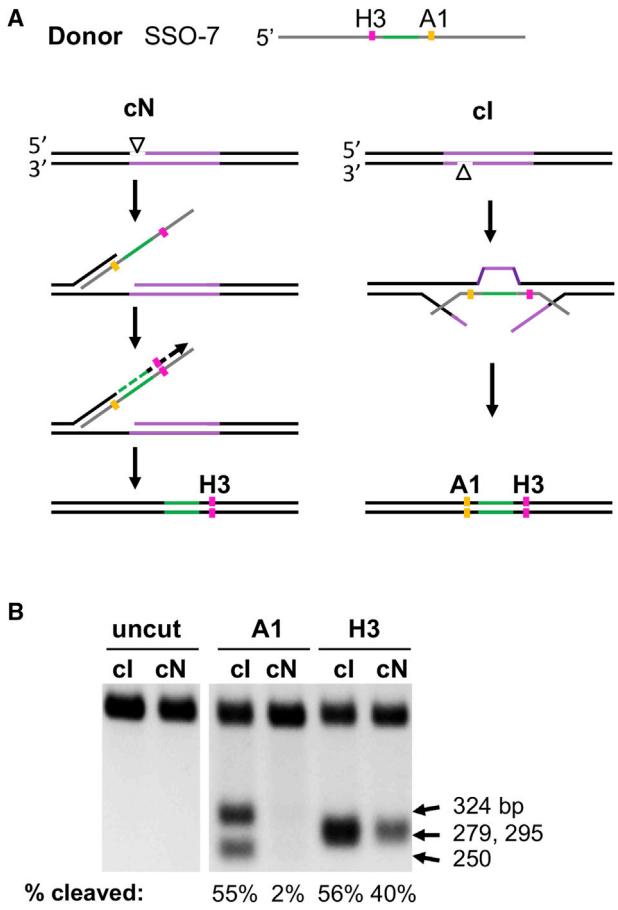

Figure 2. Unidirectional Conversion of Markers Distinguishes the cN Pathway of Gene Correction

(A) Top: diagram of HindIII (H3) and ApoI (A1) site polymorphisms on donor SSO-7. Bottom: diagram contrasting incorporation of HindIII (H3) and ApoI (A1) restriction cleavage polymorphisms into products of HDR by pathways that utilize cI or cN SSO donors.

(B) Restriction cleavage analysis of products of HDR at targeted nicks that use SSO-7 as a cI (g1) or cN (g8) donor. Fragment sizes indicated at right, percent of each fragment cleaved shown below. Approximately 2,000 independent HDR events are represented in each gel lane shown.

HDR frequencies supported by guide RNA/donor pairs that utilize the cI pathway (guide RNAs g1 or g9 and SSO-1; g2 or g8 and SSO-2) (Figure 1B) varied over a 5-fold range (0.8%–4.0%) (Figure 1E) in cells treated with siBRCA2. The highest frequency, 4.0%, was comparable to the highest frequency observed in HDR via the cN pathway. However, in contrast to the cN pathway, the cI pathway exhibited the highest HDR frequency at the site targeted by g1 and the lowest at the site targeted by g9. HDR frequencies decreased as the length of heterology on the 5′ side of the nick increased. Similar results were evident in cells treated with the control siRNA, siNT2, rather than siBRCA2 (Figure S1B). The guide RNAs assayed target nicks within or 3 nt outside of the region of heterology in the chromosomal reporter, so correction requires the cI donor to anneal to the intact strand of the target on both sides of the nick. Annealing requires that a single-stranded region be exposed by unwinding or resection of both the 3′ and 5′ ends of the nick. If the length of heterology between donor and target is increased at one side of the nick, more unwinding/resection in that direction will be required to enable annealing. Thus the reduction in HDR frequencies with increasing heterology at the 5′ side of the nick suggests that unwinding/resection is relatively less active in the 5′–3′ direction, and this limits annealing of a cI donor at the 5′ side of the nick.

Efficiencies of the cN and cI pathways appear to be comparable, provided that target/donor pairings are correctly designed. Nicks targeted to the transcribed strand undergo HDR at frequencies ~2-fold higher than nicks targeted to the non-transcribed strand, independent of pathway (Figure S1C).

Unidirectional Conversion of Markers Distinguishes the cN Pathway of Gene Correction

To test the prediction that a cN donor transfers sequence from only the donor 5′ arm, we used a 99-nt single-stranded donor, SSO-7, which carries silent single nucleotide changes that create HindIII or ApoI restriction fragment polymorphisms 5′ or 3′ of the heterology, respectively (Figure 2A). GFP^+ cells were sorted, DNA isolated, the region targeted for HDR amplified by PCR, cleaved with HindIII or ApoI, and fragments resolved by gel electrophoresis to quantify sequence conversion. SSO-7 is a cI donor at nicks targeted by g1, and a cN donor at nicks targeted by g8. In cells corrected by SSO-7 following targeting by g1, the two restriction polymorphisms were transferred with similar efficiency (ApoI 55%, HindIII 56%; Figure 2B). Conversely, in cells corrected by SSO-7 following targeting by g8, only the HindIII site was transferred at an appreciable frequency (ApoI 2%, HindIII 40%; Figure 2B). Thus, sequence conversion by cN donors is unidirectional, in clear contrast to conversion by cI donors. These results further support the view that HDR by cN donors proceeds via an annealing-driven strand synthesis pathway.

Mechanism-Based Design of Donors Improves Gene Correction Efficiency

Based on the results above (Figure 1), we predict that HDR frequencies can be improved by modifying the extent and position of donor heterology. To test this, we assayed HDR supported by 121 nt SSO donors (SSO-3, SSO-4, SSO-5, and SSO-6) that will generate a 1-nt insertion that shifts the downstream mCherry gene into the correct reading frame and enable mCherry expression (Figure 3A). These donors carry a central 39-nt region that is highly homologous to the 38-bp region in the TL reporter and span the same target sequence as SSO-1 and SSO-2 (Figure 3B). In addition to the 1-nt insertion, all donors contain three mismatches to the 38-bp region in the TL reporter to protect them and the converted target from subsequent cleavage, and SSO-5 and SSO-6 contain an additional mismatch to convert a STOP codon that would otherwise prevent mCherry expression (see aligned sequences, Figure S2). Cells were treated with siRAD51, which stimulates HDR at nicks by SSO donors but produces a relatively low background level of mutEJ ($mCherry^+$ cells), and HDR frequencies were calculated by subtracting this background as determined in the absence of exogenous

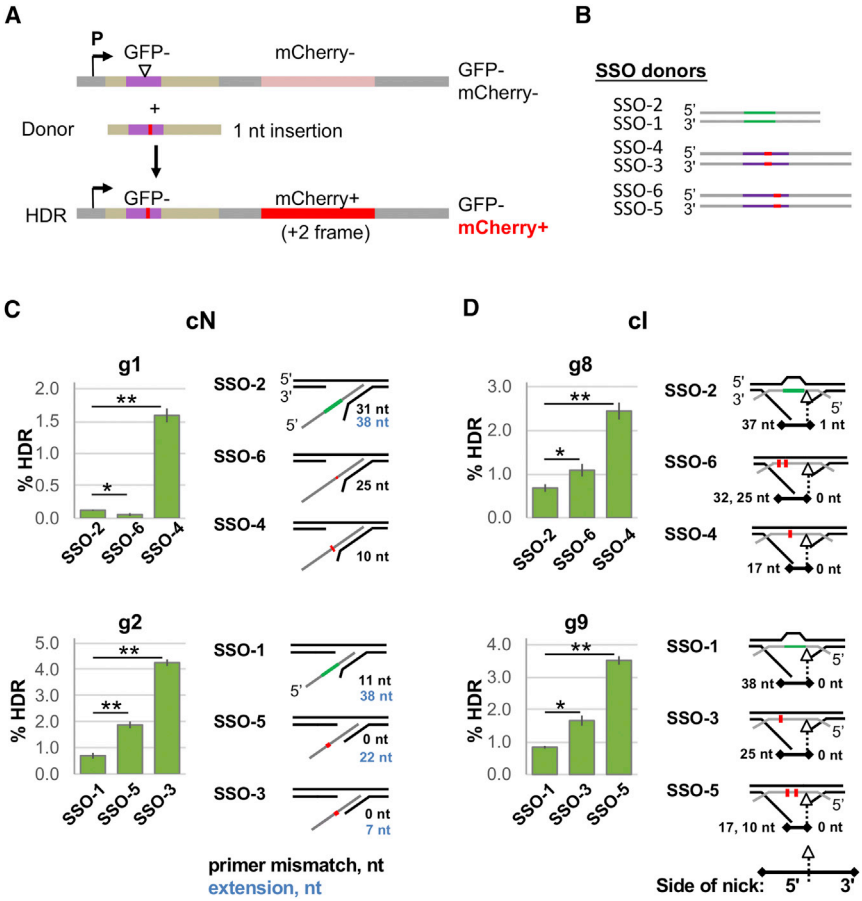

Figure 3. Effects of Donor Heterology Position on HDR Efficiency

(A) TL reporter assay of HDR by donors bearing 1-nt insertions (red) that enable mCherry expression, showing chromosomal target bearing promoter (P), defective GFP gene, and out of frame mCherry gene. Targeted nick (arrowhead) initiates repair by an HDR donor.

(B) SSO donors for HDR enabling GFP or mCherry expression, showing heterology enabling GFP expression (green) and 1-nt insertion enabling mCherry expression (red). See also Figure S2.

(C) HDR frequencies supported by indicated cN donors at nicks targeted by indicated guide RNAs. Insertions required for mCherry$^+$ expression (red), primer mismatch of the target/donor (black), and required length of extension (blue) are indicated. HDR was stimulated by knockdown of RAD51. HDR frequencies are shown as mean and SEM ($n \geq 6$, $^*p < 0.05$ and $^{**}p < 10^{-3}$, raw data presented in Data S1).

(D) HDR frequencies supported by indicated cI donors at nicks targeted by indicated guide RNAs. Insertions required for mCherry$^+$ expression (red) and heterology of the target/donor at the 5′ and 3′ sides of the nick (black) are indicated. HDR was stimulated by knockdown of RAD51. HDR frequencies are shown as mean and SEM ($n \geq 6$, $^*p < 0.05$ and $^{**}p < 10^{-3}$, raw data presented in Data S1).

donor (<0.5%) from the frequency of mCherry$^+$ cells generated in the presence of donor (Data S1).

HDR via the cN pathway at nicks targeted by g1 and supported by donors SSO-4 and SSO-6 will require 3′ excision to remove primer mismatch, as in these donors the 1-nt insertion is positioned 10 nt or 25 nt from the 3′ end of the nick. The HDR frequency was 1.6% by donor SSO-4 and 0.1% by donor SSO-4 (Figure 3C), confirming that 3′–5′ excision presents a considerable challenge for HDR. In contrast, HDR at nicks targeted by g2 and supported by donors SSO-3 and SSO-5 does not require 3′ excision of the target, but does require copying of at least 7- or 22-nt of donor sequence, respectively, to enable mCherry expression (Figure 3C). The HDR frequency was 2-fold higher with donor SSO-3 than SSO-5, highlighting the importance of the distance required for repair synthesis in determining HDR frequencies.

HDR via the cI pathway at nicks targeted by g8 and supported by donor SSO-4 will require conversion of 1 nt at a position 17 nt away from the 5′ side of the nick and supported by donor SSO-6 will require conversion of 2 nt located 25 and 32 nt away in the same direction (Figure 3B). Frequencies supported by these donors were 1.6% and 2.4%, respectively. At nicks targeted by g9, the HDR frequency was 1.7% when supported by SSO-3, which requires conversion of 1 nt located 25 nt away from the nick on the 5′ side, and 3.5% when supported by SSO-5, which requires conversion of 2 nt located 10 and 17 nt away from the nick on the 5′ side (Figure 3D). Thus, the distance from the nick to positions that require conversion, especially at the 5′ side of the nick, is an important determinant of frequency of HDR via the cI pathway.

RPA Promotes Both HDR and mutEJ at Nicks

RPA is critical for canonical HDR at DSBs, as it binds ssDNA ends exposed by resection until BRCA2 replaces it with RAD51 to enable invasion of a duplex DNA donor (Symington and Gautier, 2011). To ask whether RPA also plays a critical role at nicks, we determined the frequency of HDR with SSO donors at nicks, in cells treated with siBRCA2 and either siRPA1, which targets the largest subunit of the RPA heterotrimer, or the control non-targeting siRNA, siNT2 (Figure 4A, left). HDR frequencies were greatly reduced by siRPA1 treatment: 13.5-fold at nicks targeted by g1 and corrected by cI donor SSO-1 ($p = 1.5 \times 10^{-8}$) and 11.7-fold at nicks targeted by g9 and corrected by cN donor SSO-2 ($p = 5.7 \times 10^{-4}$). RPA depletion also reduced the frequency of HDR at nicks targeted by g1 and corrected with the dsDNA plasmid donor, pCVL SFFV d14GFP (2.7-fold, $p = 3.8 \times 10^{-5}$) and the frequency of canonical HDR at DSBs targeted by g1 and corrected by the plasmid donor (6.0-fold, $p = 3.3 \times 10^{-5}$), consistent with results of others (Wang and Haber, 2004; Chen and Wold, 2014). These results establish a key role for RPA in gene correction at nicks.

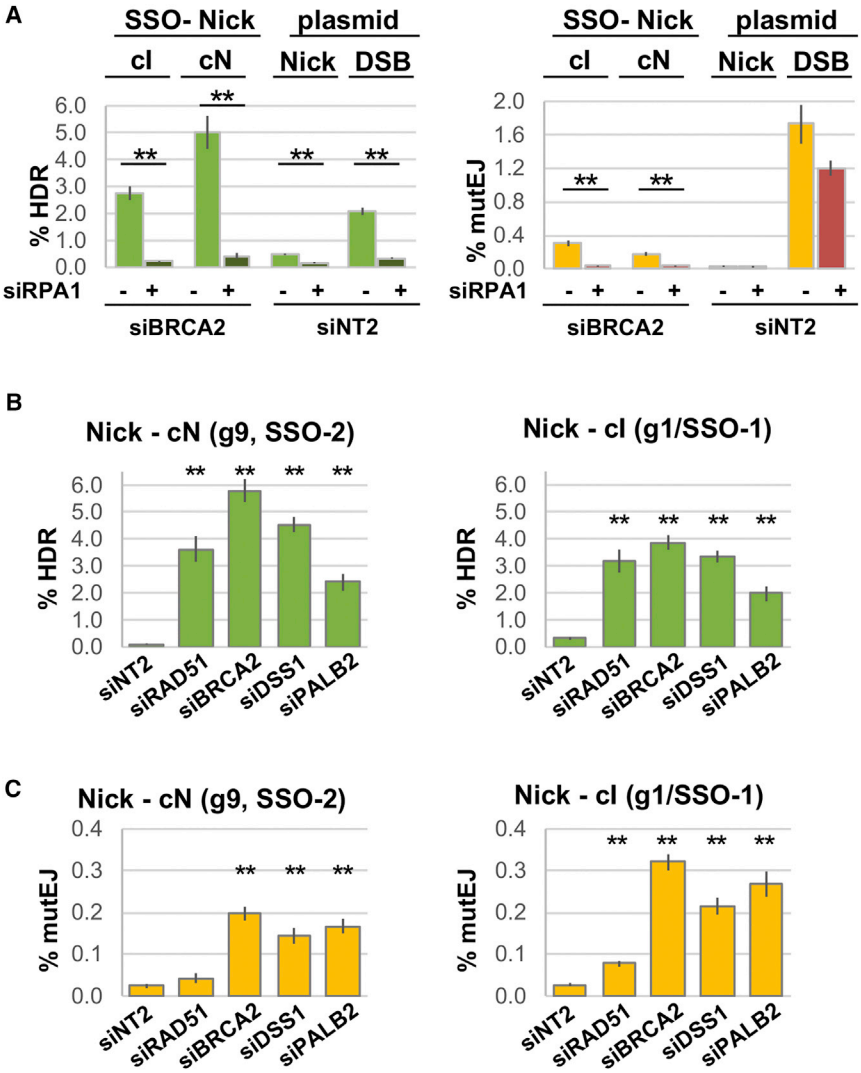

Figure 4. RPA Stimulates and RAD51 Suppresses HDR and mutEJ at Nicks

(A) HDR and mutEJ frequencies at nicks and DSBs in cells treated with the indicated siRNA. Nicks were targeted by g1 and corrected by cl donor SSO-1 or targeted by g9 and corrected by cN donor SSO-2, and nicks and DSBs were targeted by g1 for correction by the dsDNA plasmid donor, pCVL SFFV d14GFP. Frequencies are shown as mean and SEM ($n \geq 6$, $^{**}p < 10^{-3}$, raw data presented in Data S1).

(B) Frequencies of HDR at nicks by cN and cl pathways in cells treated with the indicated siRNAs to prevent RAD51 loading. Frequencies are shown as mean and SEM ($n \geq 9$, $^{**}p < 10^{-3}$ when compared to siNT2, raw data presented in Data S1). See also Figure S3.

(C) Frequencies of mutEJ at nicks in cells treated with the indicated siRNAs to prevent RAD51 loading. Frequencies are shown as mean and SEM ($n \geq 9$, $^{**}p < 10^{-3}$ when compared to siNT2, raw data presented in Data S1).

We also determined the frequency of mutEJ ($mCherry^+$ cells) in the same experiments (Figure 4A, right). In cells treated with siBRCA2, depletion of RPA1 reduced mutEJ 10.8-fold at nicks targeted by g1 ($p = 4.1 \times 10^{-7}$) and 5.9-fold at nicks targeted by g9 ($p = 9.7 \times 10^{-4}$). Strikingly, without siBRCA2 treatment, mutEJ was not significantly affected by RPA1 depletion, at either nicks or DSBs ($p = 0.90$ and 0.08, respectively). These results suggest that in the absence of BRCA2, RPA promotes mutEJ at nicks.

RAD51 Suppresses HDR by SSO Donors and mutEJ at Nicks

The RPA-dependent increase in mutEJ frequencies caused by siBRCA2 treatment (Figure 4A) suggested that BRCA2 may have previously unappreciated roles in maintaining genomic stability at nicks, possibly via its ability to load RAD51 onto RPA-coated single-stranded DNA. Because the RAD51 loading activity of BRCA2 is at least partially dependent on DSS1 and PALB2 (Prakash et al., 2015), we compared the effects of depletion of RAD51, BRCA2, DSS1, and PALB2 on HDR and mutEJ at nicks.

In assays that used the optimal target/donor pairs for the cN (g9/SSO-2) and cl (g1/SSO-1) pathways, we found that depletion of these factors stimulated HDR via the cN pathway from 19-fold (siPALB2) to 47-fold (siBRCA2) and stimulated HDR via the cl pathway from 6-fold (siPALB2) to 12-fold (siBRCA2) (Figure 4B). Control experiments showed that depletion of any of the four factors significantly reduced HDR by dsDNA donors at both nicks and DSBs (Figure S3).

Depletion of these factors also significantly increased the frequency of mutEJ at nicks. This frequency was very low in cells treated with the control siRNA, siNT2 (0.02%), and was increased by depletion from 2-fold (siRAD51) to as much as 12-fold (siBRCA2; Figure 4C). Interestingly, although depletion of RAD51 did stimulate mutEJ, stimulation was less than observed upon depletion of BRCA2, DSS1, or PALB2. Taken together, the results above suggest that the ability of DNA nicks to initiate either mutEJ or HDR by SSO donors is suppressed by loading of RAD51 onto single-stranded DNA at nicks.

At DSBs, HDR by SSO Donors Occurs Predominately by Annealing-Driven Strand Synthesis

SSO donors can support HDR at DSBs (Chen et al., 2011). To ask if this occurs by pathways related to those that support HDR at nicks, we compared HDR frequencies at DSBs targeted by g1, g2, g8, and g9 and supported by the SSO-1 or SSO-2 (Figure 5A). SSO donors supported HDR with frequencies varying over a 15-fold range, from 0.2% to 3.1% (Figure 5B). Control experiments showed that the plasmid donor supported HDR with frequencies varying over a 2.5-fold range, from 1.5% to 3.2%, and at any given DSB site, the frequencies of HDR supported by the duplex donor

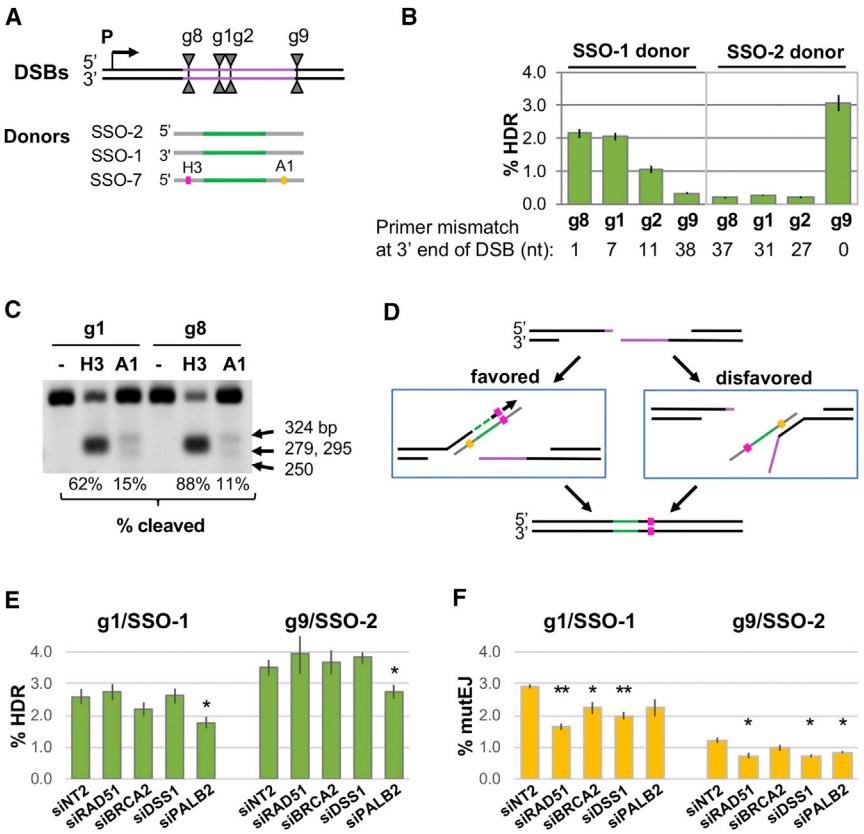

Figure 5. HDR at DSBs by SSO Donors Is Independent of RAD51 and Occurs Predominately via the ADSS Pathway

(A) Top: diagram of the TL reporter showing the region of heterology (purple) and position of DSBs targeted by gRNAs 1, 2, 8, and 9. Bottom: donors SSO-1, SSO-2, and SSO-7, showing central heterologous region (blue) flanked by homology arms (gray). ApoI (A1) and HindIII (H3) restriction polymorphisms in the SSO-7 donor are indicated.

(B) HDR frequencies at DSBs at each target/donor pair tested. Extent of primer mismatch between the SSO donor and the complementary 3′ end of each DSB is indicated below. HDR frequencies are shown as mean and SEM ($n \geq 6$, raw data presented in Data S1). Primer mismatch at 3′ end of DSB indicated below (blue). See also Figure S4.

(C) Conversion of HindIII (H3) and ApoI (A1) site polymorphisms assayed by restriction cleavage analysis of products of HDR at DSBs targeted by g1 or g8 and supported by donor SSO-7. Fragment sizes indicated at right, percent of each fragment cleaved shown below. Approximately 2,000 independent HDR events are represented in each gel lane shown.

(D) Model for HDR at a DSB via the ADSS pathway, showing resected DSB (top), annealing to SSO-7 followed by strand synthesis, indicated postulated favored and disfavored intermediates (middle), and product of HDR (bottom).

(E) Frequencies of HDR at DSBs by the indicated gRNA/donor pairs in cells treated with the indicated siRNAs to prevent RAD51 loading. Frequencies are shown as mean and SEM ($n = 6$, $^{*}p < 0.05$ and $^{**}p < 10^{-3}$ when compared to siNT2, raw data presented in Data S1).

(F) As in (E), except mutEJ frequencies are reported.

and the preferred SSO donor were not significantly different (Figure S4; Data S1). At each site, donor preference was determined by the amount of heterology between the donor and the 3′ ends of the DSB, and the preferred SSO donor was that which annealed to the 3′ end of the DSB with the least heterology and could therefore most readily prime synthesis (Figure 5B). At each of the four different DSB sites tested, the frequency of HDR supported by the preferred donor decreased as heterology with the 3′ end of the DSB increased (Figure 5B). This was also evident at nicks using cN donors (Figure 1C), where it reflects mismatch between the 3′ end of the nick that serves as a primer and the donor template. The results in Figure 5B suggested that correction of DSBs by HDRs might also exhibit unidirectional sequence conversion characteristic of the annealing-driven strand synthesis pathway that supports HDR at nicks by cN donors. To determine whether conversion at DSBs is unidirectional or bidirectional, we targeted DSBs with g1 or g8, used SSO-7 (Figure 5A) as a repair donor, sorted GFP^{+} cells and determined the frequencies of transfer of the HindIII and ApoI polymorphisms to the GFP^{+} products of HDR. The HindIII polymorphism in the donor 5′ arm was transferred much more frequently than the ApoI polymorphism in the 3′ arm (g1: 62% versus 15%; g8: 88% versus 11%; Figure 5C). Thus, sequence conversion by SSO donors at DSBs occurs predominately by an annealing-driven strand synthesis pathway, in which the 3′ arm of the donor SSO anneals to the free 3′ end of the cleaved target and is used as a template for repair synthesis (Figure 5D).

We then asked if HDR by SSOs at DSBs responded to depletion of BRCA2, RAD51, DSS1, or PALB2, testing the most efficient target/donor combinations, g1/SSO-1 and g9/SSO-2 (Figure 5E). Depletion of RAD51, BRCA2, and DSS1 did not significantly affect HDR frequencies, while depletion of PALB2 caused a modest decrease (1.5-fold, $p = 0.021$, g1/SSO-1; 1.3-fold, $p = 0.046$, g2/SSO-2). Depletion of each of these four factors caused modest (1.2- to 1.8-fold) but statistically significant reductions in mutEJ (Figure 5F). Thus, HDR by SSO donors and mutEJ at DSBs and nicks differ in their responses to RAD51 loaded on DNA.

A model for how RAD51 may suppress HDR by SSO donors and mutEJ at nicks but not DSBs is presented in Figure 6. Key to this difference are the distinct structures of recombination intermediates formed by initial processing of DSBs and nicks. A DSB undergoes extensive 5′–3′ resection to expose a 3′ single-stranded tail on both ends of the break. In contrast, a nick undergoes only limited resection but a single-stranded 3′ tail (and possibly a 5′ tail) is exposed by unwinding, as demonstrated by the inhibitory effect of heterology on the use of cN donors (Figures 1D, 1E, 3C, and 3D). RPA binds the exposed single-stranded regions at DSBs and

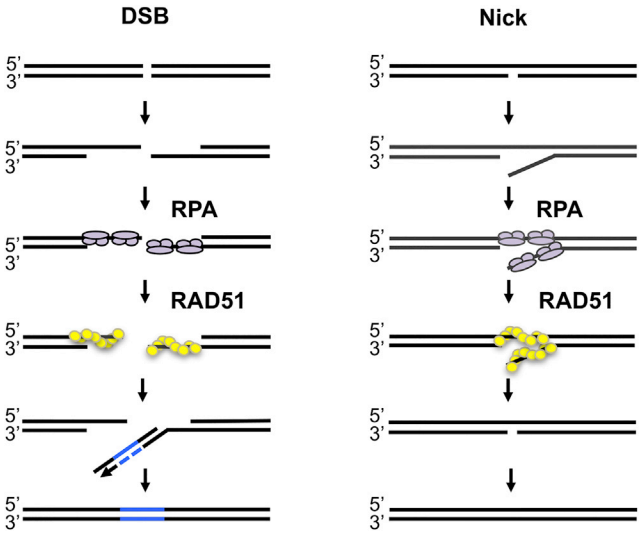

Figure 6. Suppression of HDR and mutEJ by SSOs at Nicks by RAD51

Left: a DSB undergoes 5′–3′ resection, RPA loads on the exposed single-stranded DNA, then RAD51 replaces RPA, but this does not prevent annealing by an SSO. Right: a nick is not resected but unwound at its 3′ end, RPA loads, is replaced by RAD51, then promotes reannealing of the target, thereby inhibiting HDR and mutEJ.

nicks and then is replaced by RAD51, which is loaded onto DNA by BRCA2 and its accessory factors, including DSS1 and PALB2. The RAD51-coated single-stranded 3′ tails of a resected DSB (Figure 6, left) can invade a duplex donor or anneal directly with an SSO donor, but they cannot form a duplex by reannealing with the original complementary strands because those strands have been resected. In contrast, RAD51 filaments formed on the exposed single-stranded DNA at a nick may promote re-annealing of the complementary target strands (Figure 6, right).

DISCUSSION

We have experimentally distinguished two pathways of HDR by SSO donors. The annealing-driven strand synthesis (ADSS) pathway acts at DSBs as well as at nicks. Its hallmark is unidirectional sequence transfer from the donor to the 3′ end of the target. The ADSS pathway depends on the ability of the target 3′ end to prime repair synthesis, and at nicks, it supports use of donors complementary to the nicked strand. Efficiency of the ADDS pathway is sensitive to heterology between the 3′ end of the nick or DSB and the donor, because mismatched primer termini are not efficiently extended by most DNA polymerases (Goodman et al., 1993; Kunkel, 2004). At both nicks and DSBs, the extended SSO donor must reanneal to the target to complete sequence conversion, in a step that may involve template switching or depend upon annealing activities such as RAD52.

The second pathway depends upon annealing-driven heteroduplex correction to transfer sequence from donors complementary to the intact strand of a nick. HDR via this pathway transfers sequence from the donor to sites on either side of the nick. The distance from the nick to positions that require conversion is an important determinant of efficiency, especially at the 5′ side of the nick.

Mechanism-Based Guidelines for Design of SSO Donors for HDR

Synthetic SSO donors represent a valuable alternative to duplex donors for genome engineering applications. They are convenient to synthesize, persist for a limited time in the nucleus, and their ease of production facilitates multiplexing targeted mutagenesis. Guidelines for optimizing design of SSO donors for gene correction at both targeted DSBs and nicks emerge from definition of the pathways that support their use (Figures 1A and 5D). Within any region of DNA, possible target sites are limited by the requirement for annealing of the guide RNA adjacent to a PAM site, and the orientation of the PAM site will determine the strand that will be nicked. Working within that constraint, it is critical that donors be designed specifically to support HDR via one of the two pathways. The ADSS pathway, which is active at both nicks and DSBs, transfers sequence unidirectionally and is most efficient when the 3′ end of the nick or DSB—that primes DNA synthesis—matches the donor. HDR via the cI pathway at nicks transfers sequences from a cI donor to positions on either side of the nick and is inhibited primarily by heterology at the 5′ side of the nick. Efficiencies of these two pathways appear to be comparable, provided that target/donor pairings are carefully designed.

Our results establish that cells have endogenous activities that can compensate to some extent for suboptimal target/donor pairings, although at some cost to HDR. Mismatched primer 3′ termini <10 nt in length appear to be fairly readily removed, but with accompanying reduction in HDR frequencies (Figures 1D and 3C). The heterologous 3′ ends could be removed by the 3′ flap endonuclease activity of XPF and/or MUS81-EME2 (Ciccia et al., 2008; Pepe and West, 2014) or by the 3′–5′ exonuclease activity of Polδ and/or WRN (Kamath-Loeb et al., 2012). Sequences can be transferred at a distance from the nick (Figures 1E and 3D), but with a reduction in HDR frequencies that suggests that repair may involve polymerases that are limited in the extent of synthesis, or even non-processive. Participation of these activities may differ from one cell type to another, or from one locus to another in a single cell type.

The ability of SSO donors to support HDR at DSBs has been previously examined in *S. cerevisiae*, in experiments that tested the ability of SSO donors to promote recombination initiated by cleavage by the I-SceI homing endonuclease resulting in deletion of several kb of DNA (Storici et al., 2006). Those authors favored a model in which the SSO annealed to an exposed free 3′ end at one side of the DSB and supported repair synthesis, similar to ADSS, followed by a second annealing step in which the newly extended end of the target bridged the gap to the other side of the DSB. In *S. cerevisiae*, HDR at DSBs by SSO donors was inhibited by RAD51, while in human cells it was independent of RAD51 (Figure 5E). This may reflect the somewhat different roles of HDR factors in these two eukaryotes.

The interaction of Cas9 with its DNA target may also impact the efficiency of HDR by different SSO donors at different target

sites. In vitro analyses show that Cas9 asymmetrically releases cleaved DNA ends at a DSB, as Cas9 interactions with the strand annealed to the guide RNA persist following release of one end of the opposite strand (Richardson et al., 2016). At Cas9-targeted genomic DSBs, asymmetric strand release might be evident as preferred use of SSO donors complementary to the first strand released. This was not an obvious factor in donor preference in our experiments: DSBs targeted by both g1 and g8 gave similarly high frequencies of HDR using SSO-1 as donor despite orientations predicted to favor release of opposite strands. Cas9^{D10A} nicks the strand annealed to the guide RNA and, in vitro, remains on the nicked strand while releasing the intact strand making it accessible for annealing (Richardson et al., 2016). This might suggest that targets nicked by Cas9^{D10A} would be somewhat more permissive for cI than cN donor annealing, but we did not observe a consistent difference between efficiencies of those donors that could be explained by asymmetric release of the target by Cas9^{D10A}. Instead, our results suggest that the primary contribution to HDR efficiency is the relationship between nick (or DSB) site and donor heterology.

RAD51 Suppresses Genomic Instability at Nicks

We propose (Figure 6) that RAD51 may protect nicks from both HDR and mutEJ by promoting reannealing of complementary strands at nicks. This model is based on two kinds of evidence. First, treatments that prevent RAD51 from loading onto DNA, including depletion of RAD51, BRCA2, DSS1, and PALB2, stimulate frequencies of both HDR by SSO donors and mutEJ at nicks, but not at DSBs (Figures 4B, 4C, 5E, and 5F). We propose that this is explained by the distinct structures of recombination intermediates at nicks and DSBs, as shown in Figure 6. A DSB undergoes extensive 5′–3′ resection to expose 3′ single-stranded tails. In contrast, nicks are not rapidly resected but a single-stranded 3′ tail (and possibly a 5′ tail) is exposed by unwinding, as demonstrated by the inhibitory effect of heterology on the use of cN and cI donors (Figures 1D, 1E, 3C, and 3D). Therefore, unlike DSBs, single-stranded DNA at nicks retains the ability to undergo reannealing. RAD51 may promote reannealing by displacing RPA from the single-stranded DNA. This possibility is supported by the requirement for RPA for mutEJ at nicks but not DSBs (Figure 4A, right).

The results reported here also support the view that nicks are a safer and equally effective alternative to DSBs for genome engineering. Gene correction at nicks can reach frequencies comparable to or even higher than frequencies at DSBs. Although this requires treatments that prevent RAD51 loading onto DNA, which result in a concomitant increase in mutEJ frequencies, in all conditions thus far tested frequencies of mutEJ at nicks were significantly lower than frequencies of mutEJ at DSBs (compare Figures 4C and 5F).

The results reported here also suggest an unanticipated role for RAD51 in maintenance of genomic stability by preventing mutEJ and HDR by single-stranded DNA donors at nicks. In physiological contexts, single-stranded DNA donors may be generated in the course of replication, repair, or transcription, for example by release of Okazaki fragments or unwinding associated with transcription. HDR with single-stranded DNA donors at nicks may be especially threatening to genomic stability, as it can in principle lead to short stretches of loss-of-heterozygosity. Even if HDR and mutEJ occurs with relatively low frequency at a given nick, the high frequency with which nicks occur amplifies the potential threat. This threat may be further amplified in cells deficient in RAD51 itself or factors necessary for RAD51 activity, including tumors deficient in BRCA2 or PALB2.

EXPERIMENTAL PROCEDURES

Plasmids

The pCas9^{D10A}-T2A-BFP expression plasmid was created by swapping the SpeI-SbfI fragment of pCas9^{D10A} (Davis and Maizels, 2014), which contains the D10A mutation, into the SpeI-SbfI sites of pCas9(wt)-T2A-mTagBFP (a generous gift from Dan Stetson, University of Washington, Seattle, WA).

Donor Oligonucleotides

Sequences of donor oligonucleotides are shown below, with regions that are homologous with the target in upper cases and regions of heterology in lower case. The central heterology in SSO-1, SSO-2, and SSO-7 protects them or the converted target from cleavage. SSO-3 through SSO-6 contain three mismatches to protect them or the converted target from cleavage. SSO-3 through SSO-6 also contain a 1-nt insertion and SSO-5 and SSO-6 contain an additional mismatch to destroy a STOP codon (underlined) that are necessary to permit mCherry expression.

SSO-1: 5′-CGGTGGTGCAGATGAACTTCAGGGTCAGCTTGCCGTAGGTGgcatcgccctcaccctcGCCGGACACGCTGAACTTGTGGCCGTTTACGTCGCCGTCCA-3′
SSO-2: 5′- TGGACGGCGACGTAAACGGCCACAAGTTCAGCGTGTCCGGCgagggtgagggcgatgcCACCTACGGCAAGCTGACCCTGAAGTTCATCTGCACCACCG-3′
SSO-3: 5′- CGGTGGTGCAGATGAACTTCAGGGTCAGCTTGCCGTAGGTtAGCTCTTAGCTTTACAGAGAAgACCTgCTCACGGTCcAGGCCGGACACGCTGAACTTGTGGCCGTTTACGTCGCCGTCCA-3′
SSO-4: 5′- TGGACGGCGACGTAAACGGCCACAAGTTCAGCGTGTCCGGCCTgGACCGTGAGcAGGTcTTCTCTGTAAAGCTAAGAGCTaACCTACGGCAAGCTGACCCTGAAGTTCATCTGCACCACCG-3′
SSO-5: 5′- CGGTGGTGCAGATGAACTTCAGGGTCAGCTTGCCGTAGGTtAGCTCTgTAGCTTaACAGAGAAACCTgCTCACGGTCcAGGCCGGACACGCTGAACTTGTGGCCGTTTACGTCGCCGTCCA-3′
SSO-6: 5′- TGGACGGCGACGTAAACGGCCACAAGTTCAGCGTGTCCGGCCTgGACCGTGAGcAGGTTTCTCTGTtAAGCTAcAGAGCTaACCTACGGCAAGCTGACCCTGAAGTTCATCTGCACCACCG-3′
SSO-7: 5′- CGGTGGTGCAGATGAACTTCAGGGTaAGCTTGCCGTAGGTGgcatcgccctcaccctcGCCGGACACGCTGAAtTTGTGGCCGTTTACGTCGCCGTCCA-3′

Cell Culture and Transfections

HDR was assayed in human embryonic kidney HEK293T cells stably transduced with the Traffic Light (TL) reporter, as previously described (Davis and Maizels, 2014). Cells were cultured at 37°C, 5% CO_2 in DMEM (Hyclone) supplemented with 10% fetal bovine serum (Gemini Bio-Products), 200 U/mL penicillin, 200 μg/mL streptomycin (Hyclone), and 2 mM L-glutamine (Hyclone).

Transfections were performed using Lipofectamine RNAiMAX (Life Technologies) for siRNA and Lipofectamine LTX (Life Technologies) for plasmid and SSO donors according to the manufacturer's protocol. Briefly, on day 0, 293T cells were seeded in a 96-well plate at ~4 × 10^3 cells per well in 100 μL medium. On day 1, cells were transfected with siRNAs in a mixture of 0.125 μL RNAiMAX, 0.5 μL of 0.625 μM siRNA, and 9.875 μL of OptiMEM (Life Technologies) per well. On day 2, cells were transfected with expression plasmids and SSO or duplex DNA donors for HDR, in mixes containing: 30 ng of Cas9 or Cas9^{D10A} expression plasmid, 15 ng of guide RNA (gRNA) expression plasmid, and 30 ng of pCVL SFFV d14GFP dsDNA plasmid donor (~0.08 pmol) or 2.5 pmol SSO donor and 0.24 μL Lipofectamine LTX, in 20 μL of OptiMEM, per well. In all experiments, Cas9 or Cas9^{D10A} were co-expressed

as T2A "fusions" (Yan et al., 2010) with mTagBFP (BFP) to enable identification of transfectants as BFP^+ cells. Cells were collected for analysis on day 5—while the total number of HDR events increased for several more days, the number of BFP^+ cells declined—collecting cells on day 5 allowed the BFP^+ gate to more accurately indicate transfected cells.

siRNAs assayed included siNT2, siBRCA2, and siRAD51 (ID# 4390847, s2085, and s11734, respectively; Thermo Fisher Scientific) and siDSS1 (pooled ID# SI00717927, SI00717934, SI04220986, and SI04341134; QIAGEN) and siPALB2 (pooled ID# SI04132373, SI04173582, SI04195639, and SI04241104; QIAGEN).

The efficacy of knockdown or inhibition of canonical HDR factors was confirmed by assaying the effect on canonical homologous recombination (DSB by plasmid donor) as physiological control.

Reporter Assays of HDR and mutEJ

The TL reporter (Certo et al., 2011) bears a defective GFP gene in tandem with an mCherry gene in the +2 reading frame, so neither protein is correctly expressed and cells are GFP^- $mCherry^-$. HDR that replaces a 38-bp insertion in the defective GFP gene with 17 nt of heterologous donor sequence will generate a functional GFP gene and GFP^+ cells, and indels that enable use of the +2 reading frame will generate $mCherry^+$ cells.

For flow cytometry, cells from two wells of a 96-well plate were washed with PBS, trypsinized, pooled, fixed in 2% formaldehyde, and analyzed on an LSR II flow cytometer (Becton Dickinson). Typically 50,000 events were gated for linear side scatter and forward scatter to identify cells, and cells gated for linear side scatter height and width to eliminate doublets. Cas9 or $Cas9^{D10A}$ were co-expressed with mTagBFP (BFP), and data are presented as GFP^+ and $mCherry^+$ frequencies among BFP^+ cells. GFP, mCherry, and mTagBFP fluorescence were detected with 488 nm, 561 nm, and 406 nm lasers, respectively.

Statistical Analysis

Flow cytometry data were analyzed using FlowJo (Tree Star) and frequencies were transferred to Microsoft Excel. Statistical significance was determined by two-tailed t test (Data S1). Raw data (frequencies of GFP^+ among total cells, BFP^+ and GFP^+ among BFP^+ cells) for each experiment is presented in Data S1.

Sequence Conversion Analyses

Cells were seeded at 6.4×10^4 cells per well, and transfections were carried out as above, but scaled up 16-fold. On day 3, cells were expanded into 10-cm plates, and on days 8–10 processed for live cell sorting on a Becton Dickinson Aria II flow cytometer. Sorted cells were cultured for 4–6 days, and genomic DNA was prepared (QIAGEN). The region targeted for conversion was PCR-amplified using primers SFFV-F1 (5′-CCAAGGACCTGAAATGACC-3′) and oLD7 (5′-GTCCTCCTTGAAGTCGATGC-3′), using Taq DNA polymerase and ThermoPol buffer (NEB). HindIII and ApoI digestions were performed directly in the ThermoPol buffer and DNA fragments resolved on a 1.5% agarose gel.

SUPPLEMENTAL INFORMATION

Supplemental Information includes Supplemental Experimental Procedures, four figures, and one data file and can be found with this article online at http://dx.doi.org/10.1016/j.celrep.2016.10.049.

AUTHOR CONTRIBUTIONS

L.D. conducted the experiments. L.D. and N.M. designed the experiments and wrote the paper.

ACKNOWLEDGMENTS

Research reported here was supported by US National Institutes of Health (R01 CA183967 and R21 CA190675). We thank Donna Prunkard for assistance with flow cytometry.

Received: June 7, 2016
Revised: September 12, 2016
Accepted: October 14, 2016
Published: November 8, 2016

REFERENCES

Certo, M.T., Ryu, B.Y., Annis, J.E., Garibov, M., Jarjour, J., Rawlings, D.J., and Scharenberg, A.M. (2011). Tracking genome engineering outcome at individual DNA breakpoints. Nat. Methods *8*, 671–676.

Chen, R., and Wold, M.S. (2014). Replication protein A: single-stranded DNA's first responder: dynamic DNA-interactions allow replication protein A to direct single-strand DNA intermediates into different pathways for synthesis or repair. BioEssays *36*, 1156–1161.

Chen, F., Pruett-Miller, S.M., Huang, Y., Gjoka, M., Duda, K., Taunton, J., Collingwood, T.N., Frodin, M., and Davis, G.D. (2011). High-frequency genome editing using ssDNA oligonucleotides with zinc-finger nucleases. Nat. Methods *8*, 753–755.

Ciccia, A., McDonald, N., and West, S.C. (2008). Structural and functional relationships of the XPF/MUS81 family of proteins. Annu. Rev. Biochem. *77*, 259–287.

Cong, L., Ran, F.A., Cox, D., Lin, S., Barretto, R., Habib, N., Hsu, P.D., Wu, X., Jiang, W., Marraffini, L.A., and Zhang, F. (2013). Multiplex genome engineering using CRISPR/Cas systems. Science *339*, 819–823.

Davis, L., and Maizels, N. (2011). DNA nicks promote efficient and safe targeted gene correction. PLoS ONE *6*, e23981.

Davis, L., and Maizels, N. (2014). Homology-directed repair of DNA nicks via pathways distinct from canonical double-strand break repair. Proc. Natl. Acad. Sci. USA *111*, E924–E932.

Deng, S.K., Chen, H., and Symington, L.S. (2015). Replication protein A prevents promiscuous annealing between short sequence homologies: implications for genome integrity. BioEssays *37*, 305–313.

Gasiunas, G., Barrangou, R., Horvath, P., and Siksnys, V. (2012). Cas9-crRNA ribonucleoprotein complex mediates specific DNA cleavage for adaptive immunity in bacteria. Proc. Natl. Acad. Sci. USA *109*, E2579–E2586.

Goodman, M.F., Creighton, S., Bloom, L.B., and Petruska, J. (1993). Biochemical basis of DNA replication fidelity. Crit. Rev. Biochem. Mol. Biol. *28*, 83–126.

Heyer, W.D., Ehmsen, K.T., and Liu, J. (2010). Regulation of homologous recombination in eukaryotes. Annu. Rev. Genet. *44*, 113–139.

Jinek, M., Chylinski, K., Fonfara, I., Hauer, M., Doudna, J.A., and Charpentier, E. (2012). A programmable dual-RNA-guided DNA endonuclease in adaptive bacterial immunity. Science *337*, 816–821.

Kamath-Loeb, A.S., Shen, J.C., Schmitt, M.W., and Loeb, L.A. (2012). The Werner syndrome exonuclease facilitates DNA degradation and high fidelity DNA polymerization by human DNA polymerase δ. J. Biol. Chem. *287*, 12480–12490.

Kowalczykowski, S.C. (2015). An overview of the molecular mechanisms of recombinational DNA repair. Cold Spring Harb. Perspect. Biol. *7*, a016410.

Kunkel, T.A. (2004). DNA replication fidelity. J. Biol. Chem. *279*, 16895–16898.

Mali, P., Yang, L., Esvelt, K.M., Aach, J., Guell, M., DiCarlo, J.E., Norville, J.E., and Church, G.M. (2013). RNA-guided human genome engineering via Cas9. Science *339*, 823–826.

Pepe, A., and West, S.C. (2014). Substrate specificity of the MUS81-EME2 structure selective endonuclease. Nucleic Acids Res. *42*, 3833–3845.

Prakash, R., Zhang, Y., Feng, W., and Jasin, M. (2015). Homologous recombination and human health: the roles of BRCA1, BRCA2, and associated proteins. Cold Spring Harb. Perspect. Biol. *7*, a016600.

Richardson, C.D., Ray, G.J., DeWitt, M.A., Curie, G.L., and Corn, J.E. (2016). Enhancing homology-directed genome editing by catalytically active and inactive CRISPR-Cas9 using asymmetric donor DNA. Nat. Biotechnol. *34*, 339–344.

Storici, F., Snipe, J.R., Chan, G.K., Gordenin, D.A., and Resnick, M.A. (2006). Conservative repair of a chromosomal double-strand break by single-strand DNA through two steps of annealing. Mol. Cell. Biol. *26*, 7645–7657.

Symington, L.S., and Gautier, J. (2011). Double-strand break end resection and repair pathway choice. Annu. Rev. Genet. *45*, 247–271.

Wang, X., and Haber, J.E. (2004). Role of Saccharomyces single-stranded DNA-binding protein RPA in the strand invasion step of double-strand break repair. PLoS Biol. *2*, E21.

Yan, F., Doronina, V.A., Sharma, P., and Brown, J.D. (2010). Orchestrating ribosomal activity from inside: effects of the nascent chain on the peptidyltransferase centre. Biochem. Soc. Trans. *38*, 1576–1580.